Climate Feedbacks and Their Implications for Poleward Energy Flux Changes in a Warming Climate

MARK D. ZELINKA

Department of Atmospheric Sciences, University of Washington, Seattle, Washington, and Program for Climate Model Diagnosis and Intercomparison, Lawrence Livermore National Laboratory, Livermore, California

DENNIS L. HARTMANN

Department of Atmospheric Sciences, University of Washington, Seattle, Washington

(Manuscript received 16 February 2011, in final form 24 June 2011)

ABSTRACT

Feedbacks determine the efficiency with which the climate system comes back into equilibrium in response to a radiative perturbation. Although feedbacks are integrated quantities, the processes from which they arise have rich spatial structures that alter the distribution of top of atmosphere (TOA) net radiation. Here, the authors investigate the implications of the structure of climate feedbacks for the change in poleward energy transport as the planet warms over the twenty-first century in a suite of GCMs. Using radiative kernels that describe the TOA radiative response to small perturbations in temperature, water vapor, and surface albedo, the change in poleward energy flux is partitioned into the individual feedbacks that cause it.

This study finds that latitudinal gradients in the sum of climate feedbacks reinforce the preexisting latitudinal gradient in TOA net radiation, requiring that the climate system transport more energy to the poles on a warming planet. This is primarily due to structure of the water vapor and cloud feedbacks, which are strongly positive at low latitudes and decrease dramatically with increasing latitude. Using the change in surface fluxes, the authors partition the anomalous poleward energy flux between the atmosphere and ocean and find that reduced heat flux from the high-latitude ocean further amplifies the equator-to-pole gradient in atmospheric energy loss. This implied reduction in oceanic poleward energy flux requires the atmosphere to increase its share of the total poleward energy transport. As is the case for climate sensitivity, the largest source of intermodel spread in the change in poleward energy transport can be attributed to the shortwave cloud feedback.

1. Introduction

In the global mean, the amount of energy received at the top of atmosphere (TOA) from the sun is nearly balanced by the amount of longwave (LW) energy emitted by the planet. However, this balance does not hold at every location on the planet. Absorbed shortwave (SW) radiation is large in the tropics and decreases with latitude because of the sphericity of the earth and the latitudinal gradient of planetary albedo. Because the atmosphere and ocean transport energy poleward, the meridional temperature gradient is less than if every location on the planet were in local radiative equilibrium. Thus, outgoing longwave radiation (OLR) decreases much less dramatically with latitude than absorbed solar radiation. This results in a net surplus of TOA radiation in the tropics where absorbed SW radiation exceeds OLR and a deficit at high latitudes where OLR exceeds absorbed SW radiation.

The atmosphere and ocean transport energy from the tropical regions of surplus to the extratropical regions of deficit. As such, poleward energy fluxes are fundamentally tied to the top of atmosphere radiation budget. Poleward energy transport peaks at about 5.5 PW at 35° latitude in either hemisphere, with the atmosphere accounting for 78% of the Northern Hemisphere (NH) peak and 92% of the Southern Hemisphere (SH) peak (Trenberth and Caron 2001). The atmospheric contribution to poleward energy transport dominates over the oceanic contribution at all latitudes except between the

Corresponding author address: Mark D. Zelinka, Program for Climate Model Diagnosis and Intercomparison, Lawrence Livermore National Laboratory, 7000 East Avenue, L-103, Livermore, CA 94551.
E-mail: zelinka1@llnl.gov

DOI: 10.1175/JCLI-D-11-00096.1

equator and roughly 17°N. Heat flux divergence out of the tropics is equal to the net TOA energy surplus, and energy flux convergence into the extratropics is equal to the net TOA energy deficit.

The net radiation balance at the top of the atmosphere must be adjusted to the ability of the internal dynamics of the atmosphere and ocean to transport energy poleward. Held and Soden (2006) have shown that increased poleward energy flux is a robust feature of GCM simulations of global warming. One can argue that the atmospheric meridional energy flux increases because the gradient in moist static energy increases, as Hwang and Frierson (2010) have done, but one must also ask what diabatic processes maintain that larger gradient in moist static energy. Here, we examine those diabatic processes and their change with global-mean temperature to better elucidate their critical role in inducing increased poleward energy transport in a warmed earth. The internal dynamics of the atmosphere and ocean that determine their energy flux and the radiative–convective feedback processes that maintain the meridional heating gradients are essential to the climate response that produces increased energy fluxes in a warmed earth. Here, we emphasize the latter and raise the question of which of these processes has a stronger role in determining the outcome of enhanced poleward energy flux.

Just as net TOA radiation has nonuniform spatial structure in the mean state, so does its anomaly in a warming climate. Because of the strong constraint of energy conservation in the climate system, this structure in anomalous net radiation must be associated with an anomalous poleward energy transport. Wu et al. (2010) have performed an extensive analysis of the change in poleward energy transports in the Geophysical Fluid Dynamics Laboratory Climate Model version 2.1 (GFDL CM2.1) and have related them to the TOA and surface energy budget changes. They demonstrated that a warming climate is associated with anomalous energy gain in the tropical atmosphere relative to the high-latitude atmosphere, requiring larger atmospheric poleward transport that is accomplished in part by stronger midlatitude eddies. They show that this enhanced equator-to-pole energy gradient in a warming world is associated with positive water vapor and cloud feedbacks in the tropics, negative cloud feedback at high latitudes, enhanced heat uptake by the Southern Ocean, and increased emission to space in the northern high latitudes.

This work extends the work of Wu et al. (2010) to assess the changes in TOA and surface radiation and their implications for changes in poleward energy transport in a suite of GCM simulations performed as part of the Coupled Model Intercomparison Project phase 3 (CMIP3). A unique feature of this study is the use of radiative kernels (Soden et al. 2008) to partition TOA radiative flux anomalies and their implied poleward energy transport anomalies into specific feedbacks in the climate system. Such an approach is appealing because it allows us to separate those aspects that are robust and well constrained from those that are less robust and more poorly constrained across models. Our results in general support those of Wu et al. (2010) and strengthen the claim that water vapor and cloud feedbacks in the climate system act not only to amplify the global-mean surface temperature response to CO_2 forcing but also to increase the poleward energy transport by the climate system as the planet warms. Furthermore, intermodel spread in the magnitude and spatial structure of cloud feedback (primarily SW cloud feedback) results in intermodel spread in the implied poleward energy transport accompanying global warming. Finally, it is clear from our results that feedback processes affect both the magnitude of global warming and its spatial structure, so that localized feedbacks affect the climate everywhere.

2. Data

We make use of global monthly-mean profiles of temperature and humidity, surface temperature, surface and TOA radiative fluxes in both clear- and all-sky conditions, and surface latent and sensible heat flux from 12 GCMs in the in the World Climate Research Programme's (WCRP's) CMIP3 multimodel dataset (cf. Table 1).

We compute anomalies of these quantities as the difference in the monthly-mean annual cycle of the last 10 years of the twenty-first century in the Special Report on Emissions Scenarios (SRES) A2 emissions scenario simulations and the monthly-mean annual cycle of a 30-yr climatology computed for the end of the corresponding twentieth-century (20c3m) simulations. We use the radiative kernels provided by B. J. Soden and regrid all the model data from each model's native grid onto the same grid as that of the radiative kernels (Soden et al. 2008). A total of 12 models archived enough data to permit the kernel calculation. Nine of these models archive enough surface flux data to permit partitioning the poleward flux anomalies between atmosphere and ocean (Table 1).

3. Methodology

The total change in radiation at the top of the atmosphere over the course of the century can be expressed as

$$dR = \Delta\overline{T_s}(f_T + f_q + f_\alpha + f_c) + G, \qquad (1)$$

where $\Delta\overline{T_s}$ is the change in global-mean surface temperature over the century; f_T, f_q, f_α, and f_c are the

TABLE 1. Global climate models that simulated the SRES A2 scenario and submitted sufficient data to the CMIP3 archive to permit computation of feedbacks using radiative kernels. Asterisks denote models for which all TOA fluxes are provided but at least one surface flux is not provided. Partitioning of poleward energy transport between ocean and atmosphere cannot be performed without surface fluxes.

Abbreviation	Modeling Center	Country
L'Institut Pierre-Simon Laplace Coupled Model, version 4 (IPSL CM4)	L'Institut Pierre-Simon Laplace	France
Max Planck Institute (MPI) ECHAM5	Max Planck Institute for Meteorology	Germany
Canadian Centre for Climate Modelling and Analysis (CCCma) Coupled General Circulation Model, version (CGCM3.1)	Canadian Centre for Climate Modeling and Analysis	Canada
Meteorological Research Institute Coupled General Circulation Model, version 2.3.2a (MRI CGCM2.3.2a)	Meteorological Research Institute	Japan
Met Office (UKMO) third climate configuration of the Met Office Unified Model (HadCM3)	Hadley Centre for Climate Prediction and Research/Met Office	United Kingdom
Geophysical Fluid Dynamics Laboratory Climate Model version 2.0 (GFDL CM2.0)	National Oceanic and Atmospheric Administration (NOAA)/Geophysical Fluid Dynamics Laboratory	United States
Institute of Numerical Mathematics Coupled Model, version 3.0 (INM-CM3.0)	Institute for Numerical Mathematics	Russia
Model for Interdisciplinary Research on Climate 3.2, medium-resolution version [MIROC3.2(medres)]	Center for Climate System Research (The University of Tokyo), National Institute for Environmental Studies, and Frontier Research Center for Global Change	Japan
NCAR Community Climate System Model, version 3 (CCSM3)	National Center for Atmospheric Research (NCAR)	United States
GFDL CM2.1*	NOAA/Geophysical Fluid Dynamics Laboratory	United States
NCAR PCM1*	National Center for Atmospheric Research	United States
Goddard Institute for Space Studies Model E-R (GISS-ER)*	National Aeronautics and Space Administration (NASA)/Goddard Institute for Space Studies	United States

radiative feedbacks resulting from changes in temperature T, water vapor q, surface albedo α, and clouds c, respectively; and G is the radiative forcing in the A2 scenario. In equilibrium, dR is zero by definition. The individual radiative feedbacks (with the exception of clouds) are calculated as

$$f_x = \frac{\partial R}{\partial x}\frac{dx}{d\overline{T}_s} \equiv K_x \frac{dx}{d\overline{T}_s}. \quad (2)$$

Here, K_x represents the radiative kernel, which expresses the change in TOA radiative flux due to small perturbations in variable x (Soden et al. 2008). Radiative kernels represent the LW or SW radiative response at the top of atmosphere to temperature, humidity, or surface albedo perturbations at each latitude, longitude, pressure (if applicable), and time. Each kernel is a four-dimensional matrix (latitude, longitude, pressure, and month) that is multiplied by the actual model-produced change in variable x and integrated in the vertical to calculate the total TOA flux response. Integration is performed from the surface up to a level that linearly decreases with latitude from 100 hPa at the equator to 300 hPa at the poles, in accordance with Soden et al. (2008). The feedback is computed by dividing the TOA flux response by the change in global-mean surface temperature. (For surface albedo feedback, vertical integration is not necessary.)

Cloud feedbacks are computed by adjusting the change in cloud radiative forcing (defined as the difference between clear-sky and all-sky LW, SW, or net radiative flux at TOA) by the amount of cloud masking in the other feedbacks [Eq. (25) of Soden et al. (2008)]. The cloud masking is calculated by differencing the clear- and all-sky feedbacks and adding a term due to the cloud masking of the radiative forcing G in the A2 scenario. We assume that clouds mask the radiative forcing in the SRES A2 scenario by 16%, which is the amount that the GFDL model's radiative forcing due to a doubling of CO_2 is masked by clouds (Soden et al. 2008). For the last decade of the twenty-first century, the global-mean LW and SW radiative forcings in the A2 scenario are 6.16 and -0.11 W m^{-2}, respectively [cf. Tables 6.14 and 6.15 of Ramaswamy et al. (2001)]. Thus the 16% cloud masking of the radiative forcing requires the addition of 0.99 W m^{-2} to the change in LW cloud forcing and the subtraction of 0.02 W m^{-2} from the change in SW cloud forcing to calculate the respective cloud feedbacks.

Note that the feedbacks computed here are defined more loosely than the formal definition (e.g., Hansen et al.

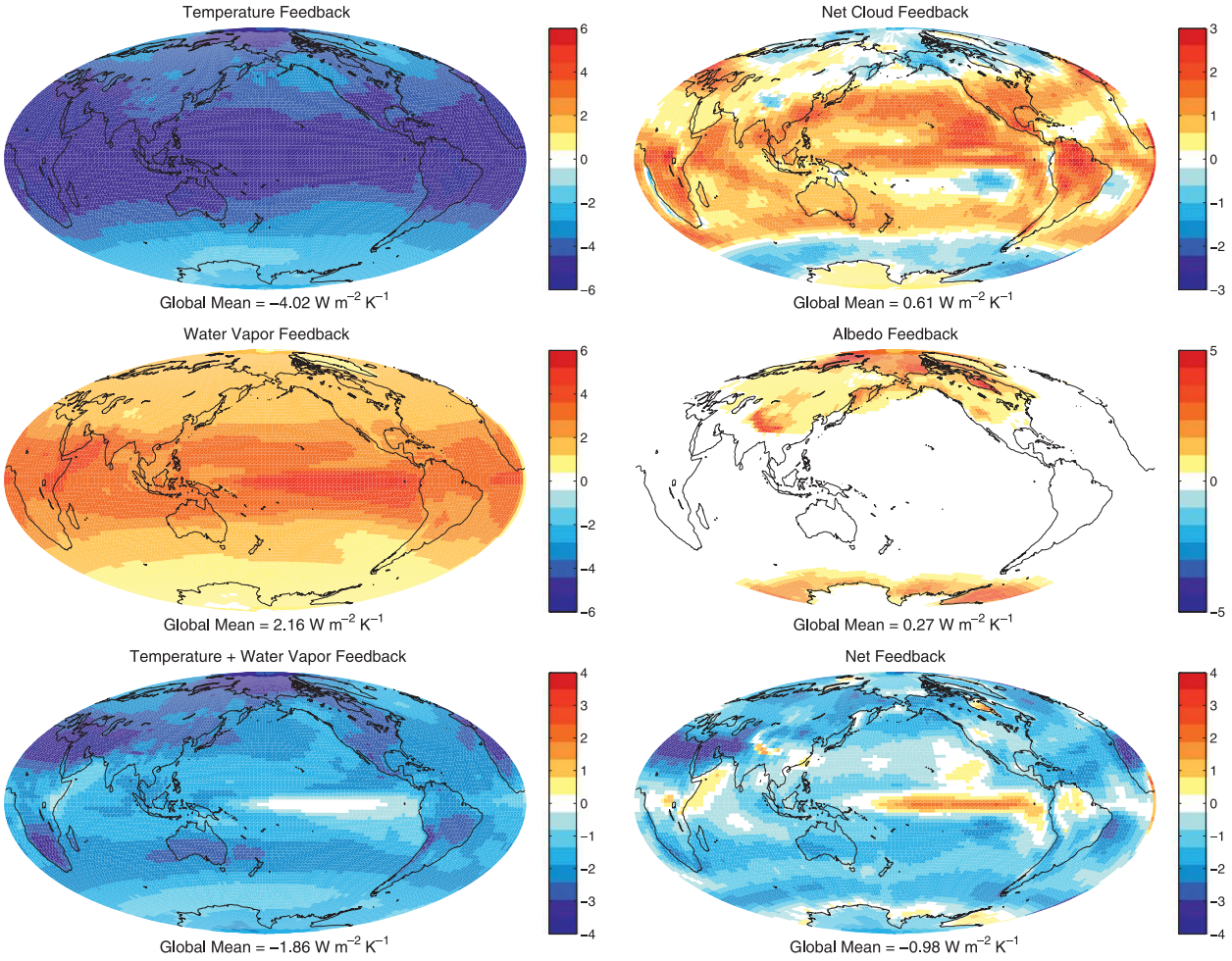

FIG. 1. Ensemble-mean temperature, water vapor, cloud, and surface albedo feedbacks, along with the combined temperature–water vapor feedback and the sum of all feedbacks computed using the kernel technique. Note that the color scales vary among panels.

1984) because we use differences between two transient climate states rather than between two equilibrium states. Also, unlike the formulation of Roe and Baker (2007) and Roe (2009) in which feedbacks are computed relative to a reference system with vertically uniform warming that is considered the basic response of the planet to increased radiative forcing (i.e., the Planck response), we refer to TOA flux anomalies owing to the full temperature response as a feedback. It is acceptable to consider the Planck response a feedback because it alters (i.e., feeds back on) the net radiative imbalance at the top of the atmosphere in a manner proportional to the amount of global-mean warming when earth is subjected to a radiative perturbation (i.e., it decreases the imbalance by causing the warmer earth to emit more LW radiation). Furthermore, because our goal is to partition anomalies in the radiation budget into components, it is necessary to include the radiative response arising from the full 3D temperature change among them. Thus our global feedback values sum to a negative number, indicating that the planet is stable with respect to radiative perturbations.

4. Spatial structure of climate feedbacks

The ensemble-mean temperature, water vapor, surface albedo, and cloud feedbacks, along with the combined temperature–water vapor feedback and the sum of all feedbacks are shown in Fig. 1. The spatial patterns and global-mean values of the feedbacks are comparable with those for the A1B scenario given in Fig. 8 of Soden et al. (2008). The temperature (lapse rate plus Planck) feedback is negative everywhere, indicating that warming the planet causes it to emit more radiation. The feedback is most negative in the tropics where the upper troposphere warms substantially, over the continents where surface warming is large, and in the Arctic where heating is confined near the surface by large lower-tropospheric stability and sea ice loss (Hansen et al.

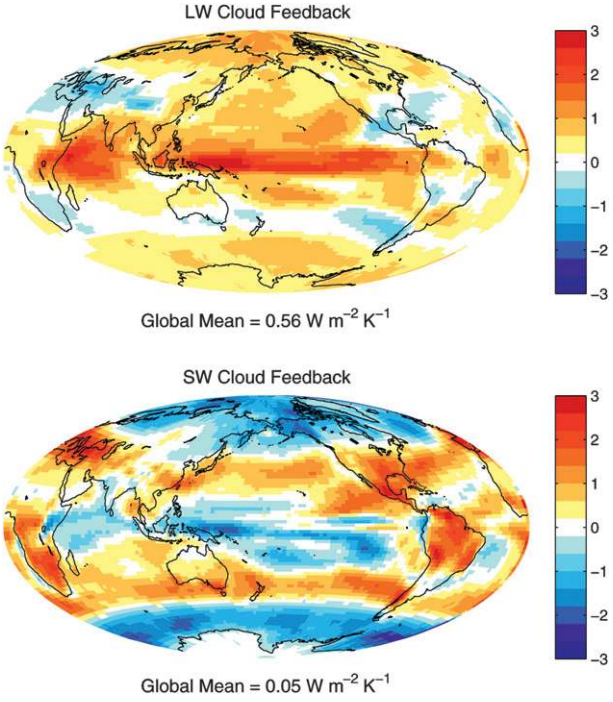

FIG. 2. Ensemble-mean LW and SW cloud feedbacks computed by adjusting the change in cloud radiative forcings as described in the text.

1984). The feedback is less negative over the Southern Ocean, where the warming is delayed relative to the rest of the planet.

The water vapor feedback is positive everywhere, with nearly constant relative humidity implying an exponential increase in the absolute abundance of water vapor as the atmosphere warms. This feedback is especially strong in the tropics due to large fractional increases in humidity that accompany warming in the climatologically dry upper troposphere. As discussed in Soden and Held (2006), large fractional increases in absolute humidity in the tropical upper troposphere are caused by a combination of the large sensitivity of saturation vapor pressure to temperature at very cold temperatures and low pressures (e.g., 15% K^{-1} at 200 K) as well as the fact that the upper troposphere warms considerably more than the surface due to the maintenance of the moist adiabatic tropical temperature profile as the planet warms.

Cloud feedback is positive (negative) at nearly every location equatorward (poleward) of 45°. This feedback is broken down into its LW and SW components in Fig. 2. The LW cloud feedback is positive nearly everywhere but is especially large where high cloud fraction increases. Zelinka and Hartmann (2010) have shown that the upward shift of high clouds in the tropics contributes significantly to the positive LW cloud feedback since high clouds maintain an almost constant temperature as the surface warms, in agreement with theoretical expectations (Hartmann and Larson 2002). SW cloud feedback is positive throughout the subtropics and negative along the equator and at high latitudes in a pattern that follows the changes in total cloud amount (not shown).

The surface albedo feedback is positive and confined to high latitudes, as expected intuitively. The larger fractional coverage of land and therefore greater snow albedo feedback in the NH results in a positive surface albedo feedback that extends to lower latitudes than in the SH.

The sum of all feedbacks when integrated over the entire planet is -1 W m^{-2} K^{-1}, indicating a climate that is stable to perturbations, though significantly less stable than a blackbody planet with no atmospheric feedbacks other than the basic Planck feedback of about -3.2 W m^{-2} K^{-1} (Hansen et al. 1984; Colman 2003; Soden and Held 2006). Quite remarkably, the net feedback map exhibits positive values along the equator in the Pacific. This locally positive net feedback is due to the combination of strong positive water vapor and cloud feedbacks. The latitudinal structure of the feedbacks will be discussed in much greater detail below.

Before continuing it is first necessary to discuss the accuracy of Eq. (1). First, this equation assumes that the radiative impact of each component change is independent of the others such that feedbacks can be added linearly to produce the TOA radiative flux anomaly, effectively ignoring interactions among feedbacks that can be important (Huybers 2010). Second, the accuracy of the equation is compromised by incomplete knowledge of the forcing term G. While global-mean radiative forcing due to long-lived greenhouse gases and sulfate aerosol concentrations is prescribed in the A2 scenario, the total radiative forcing as well as its spatial and temporal structure vary from model to model because modeling centers made use of emissions projections from different socioeconomic models (IAMs), made varying assumptions about emissions not provided by the IAMs, and included to varying degrees physical processes like aerosol indirect effects in their simulations (Shindell et al. 2008). Because neither total radiative forcing nor its spatial structure is archived for the models, our use of a G that is invariant in space and across models introduces error to the calculation. Third, one should not expect exact agreement between kernel-computed and model-generated TOA flux anomalies because the sensitivities of TOA radiation to small perturbations (i.e., the kernels) are generated using the GFDL model code and are then applied across the ensemble of models. Moreover, the mean state cloud fields in the GFDL model are different from those in the other models, which introduce error into the cloud-masking adjustments. Finally, the individual feedback terms as defined in Eq. (2) are assumed to

represent radiative flux anomalies due to component changes that are linear functions of global-mean temperature changes. Gregory and Webb (2008) have suggested that cloud cover responds directly to increased CO_2 such that an appreciable portion of the cloud-induced radiative response commonly included as part of the cloud feedback is not temperature mediated. Andrews and Forster (2008) and Colman and McAvaney (2011) found that such semidirect effects of CO_2 impact the interpretation of cloud feedback more than other feedbacks. As we have not separated the CO_2-induced and temperature-induced cloud changes (and are aware of no methodology to do so in runs with time-varying forcing), both the sign and magnitude of the cloud feedback we have calculated may be different from the true, temperature-mediated cloud feedback. All of these effects likely contribute to discrepancies between dR calculated using Eq. (1) and the model-produced dR.

Generally, when compared with actual model-produced TOA radiation flux anomalies at the end of the twenty-first century, kernel-derived estimates exhibit less LW cooling of the planet, though the opposite is the case over specific regions in some models (not shown). In contrast, the actual model-produced downwelling SW flux anomalies are more positive than the kernel-derived SW flux anomalies nearly everywhere in every model. This feature is generally larger in the NH and especially over the continents, possibly indicating regional reductions in reflective aerosols that enhance the warming relative to what is predicted from using a spatially uniform SW radiative forcing in Eq. (1). The GFDL models in particular exhibit the largest increase in actual absorbed SW radiation relative to what is predicted by Eq. (1) (not shown), consistent with the large NH radiative forcing due to short-lived species shown in Fig. 4 of Shindell et al. (2008).

5. Zonal-mean structure of climate feedbacks

In Fig. 3 we show the zonal-mean temperature, water vapor, cloud, and surface albedo feedbacks, along with the combined temperature–water vapor and sum of all feedbacks for the 12 models that archive enough data and for the multimodel mean. Water vapor feedback is greatest in the tropics and declines from approximately 4 W m^{-2} K^{-1} at the equator to 1 W m^{-2} K^{-1} at the poles (Fig. 3b). This gradient is almost completely offset at most latitudes by the temperature (Planck plus lapse rate) feedback, which is -5 W m^{-2} K^{-1} in the tropics and decreases monotonically to about -2 W m^{-2} K^{-1} in the Antarctic (Fig. 3a). Interesting hemispheric asymmetry is present in the temperature feedback because of the delayed warming in southern high latitudes and strong polar amplification of surface warming in the NH. The temperature feedback weakens to about -3.5 W m^{-2} K^{-1} at 55°N, and then it strengthens to -5 W m^{-2} K^{-1} over the North Pole.

The net water vapor plus temperature feedback thus has a weak pole-to-pole gradient with a stronger negative feedback in the NH compared to the SH (Fig. 3c). The hemispheric asymmetry can be understood to zeroth order simply by considering geography: the SH has a little over twice as much ocean area as does the NH [cf. Fig. 1.12 of Hartmann (1994)] and a robust feature of GCM simulations is that the land heats up much more than the ocean by the end of the century (Meehl et al. 2007). The exact reason for this surface warming pattern, however, remains a subject of debate in the literature (e.g., Sutton et al. 2007; Joshi et al. 2008; Dong et al. 2009) Certainly, vigorous vertical mixing in the Southern Ocean allows for large heat uptake and storage away from the surface, delaying the greenhouse gas–induced warming in this region.

The combined temperature and water vapor feedbacks exhibit significantly reduced intermodel spread at all latitudes than either feedback taken alone. Compensation of lapse rate and water vapor feedbacks is expected if relative humidity remains approximately constant (Cess 1975) and is especially significant in the tropics where temperature and humidity variations in the upper troposphere are large. Thus, models with strong negative lapse rate feedbacks (i.e., large tropical upper tropospheric warming) are also models with strong positive water vapor feedbacks such that the combination of the two feedbacks exhibits less intermodel spread than either taken alone (Soden and Held 2006).

Net cloud feedback is positive (approximately 1 W m^{-2} K^{-1}) between 50°N and 50°S and is negative in high latitudes Fig. 3d). As in the globally integrated case, the intermodel spread in total feedback at each latitude is dominated by the intermodel spread in cloud feedback. In Fig. 4 we separate the cloud feedback into its LW and SW components. It is clear that the spread in SW cloud feedback estimates are much larger at all latitudes than the spread in LW cloud feedback estimates. Furthermore, the LW cloud feedback is robustly positive across all models in the deep tropics, and only a few models exhibit negative LW cloud feedbacks at any latitude. Zelinka and Hartmann (2010) showed that the robustly positive tropical LW cloud feedback is simply due to the fact that tropical high clouds rise as the climate warms, and that models capture this because it arises as a fundamental result of radiative–convective equilibrium. Zelinka et al. (2012) show for a different ensemble of models that the positive LW cloud feedback at all latitudes—including the extratropics—is primarily

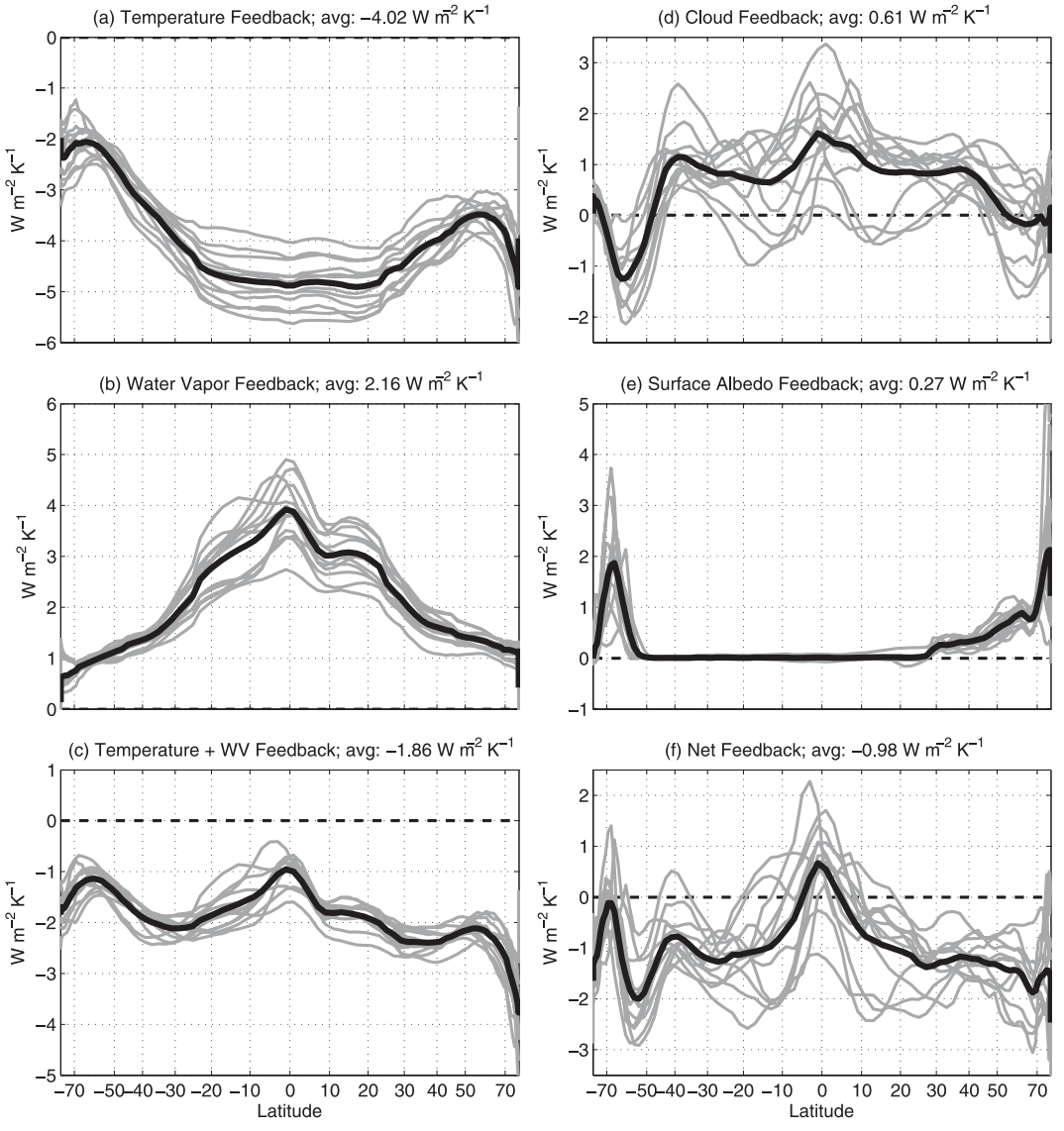

FIG. 3. Zonal-mean (a) temperature, (b) water vapor, (c) combined temperature–water vapor, (d) cloud, and (e) surface albedo feedbacks, along with (f) the sum of all feedbacks. Each of the 12 models is represented by an individual gray line, and the thick black line represents the multimodel mean. The abscissa is sine of latitude so that the visual integral is proportional to watts per kelvin of mean surface temperature change. Note that the vertical axis limits vary among panels, but all span a range of 6 W m^{-2} K^{-1}.

caused by increasing cloud altitude. The deep tropics experience the largest positive LW cloud feedback because the ensemble-mean SST and corresponding deep convection anomalies shift onto the equator in the A2 scenario in a pattern reminiscent of a permanent warm phase El Niño (Meehl et al. 2007).

A robust aspect of the SW cloud feedback structure is a transition from positive values to negative values in the extratropics, with a zero crossing near 50° in both hemispheres in the ensemble mean. This is especially apparent in the more zonally symmetric SH extratropics. Zelinka et al. (2012) demonstrate using a different ensemble of GCMs that the enhanced SW reflection poleward of 50° is a manifestation of both increased amount and optical thickness of clouds, the latter being the dominant contributor.

The global average net feedback is -1 W m^{-2} K^{-1}. In the subtropics and extratropics the net feedback is about -1.5 W m^{-2} K^{-1}, with significant intermodel variance that is primarily attributable to variance in SW cloud feedback. Interestingly, the ensemble-mean sum of all feedbacks is positive at the equator, indicating a climate that is locally unstable (Fig. 3f). That is, as the planet warms because of the long-lived greenhouse gas

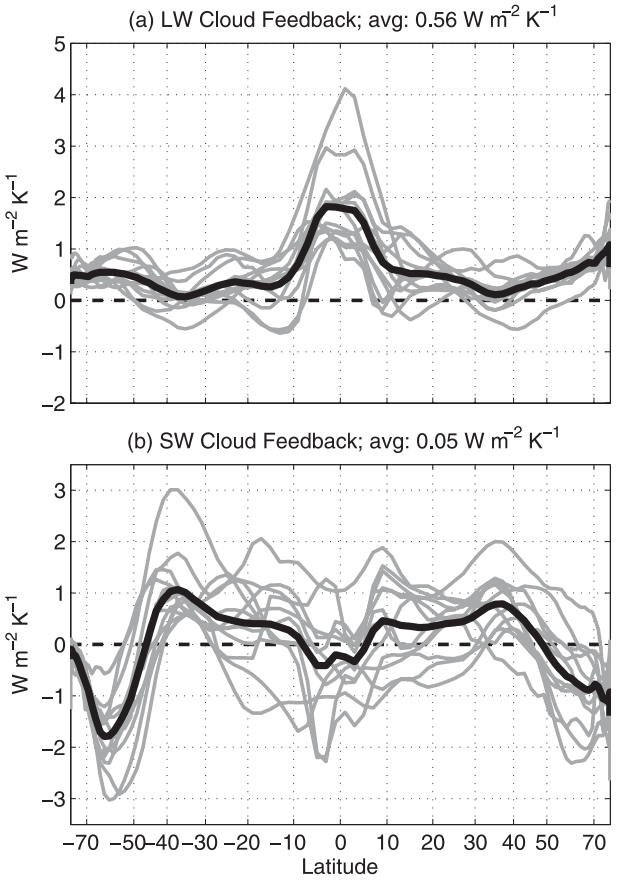

FIG. 4. As in Fig. 3, but for the (a) LW and (b) SW cloud feedbacks. Note that the vertical axis limits vary among panels, but both span a range of 7 W m^{-2} K^{-1}.

forcing, the atmospheric feedbacks act to increase the net radiative energy flux into the tropics. This net positive feedback at the equator is due to a combination of weak temperature plus water vapor feedback and strong positive cloud feedback. The net feedback decreases from positive to negative with increasing latitude following the gradient in water vapor and cloud feedbacks. Notably strong ensemble-mean negative net feedbacks are a result of strong negative cloud feedbacks at high southern latitudes and increased emission to space due to the enhanced warming of the lower troposphere at high northern latitudes.

Discussion

We consider several of the feedback response structures to be robust features of a warming climate that any model should capture regardless of parameterization. First, there are several reasons to expect an equator-to-pole gradient in the water vapor feedback.

(i) The sensitivity of OLR to water vapor perturbations (as indicated by the LW water vapor radiative kernel) is greatest in the tropical upper troposphere and decreases with latitude. Thus, the equator-to-pole gradient would exist even if fractional increases in atmospheric moisture were spatially uniform.

(ii) The Clausius–Clapeyron relation exhibits a high sensitivity of saturation vapor pressure e_s to temperature at very cold temperatures and low pressures (e.g., e_s increases 15% K^{-1} at 200 K compared to only 6% K^{-1} at 300 K). Thus, even if temperature increased uniformly everywhere and relative humidity did not change, the largest fractional increase in absolute humidity would be in the tropical upper troposphere.

(iii) It is well accepted that tropical temperatures tend to follow the moist adiabat, resulting in upper-tropospheric amplification of warming. Thus, assuming relative humidity is constant, enhanced moistening in the tropical upper troposphere would occur even in the absence of nonlinearities in the Clausius–Clapeyron relation.

Second, there are many features of the cloud response to warming that are consistent with theory, observations, and the results of simple models.

(i) A strongly positive LW cloud feedback arises because cloud-top altitude robustly increases in models following the theoretically expected rise of the level of peak radiatively driven divergence in the tropics (Hartmann and Larson 2002; Zelinka and Hartmann 2010) and of the tropopause level in the extratropics (Kushner et al. 2001; Santer et al. 2003; Lorenz and DeWeaver 2007).

(ii) Numerous observational studies (e.g., Tselioudis et al. 1992; Tselioudis and Rossow 1994; Chang and Coakley 2007) have found that cloud optical thickness decreases with temperature for clouds warmer than 0°C and increases with temperature for clouds colder than 0°C. Zelinka et al. (2012) have found optical depth changes in GCMs that are qualitatively consistent with these observed relationships and have shown a significant positive contribution to LW cloud feedback from the increasing optical depth of high tropical clouds, a positive contribution to SW cloud feedback from decreasing optical depth of low clouds equatorward of about 40°, and a very strong negative SW optical depth feedback at high latitudes. The latter feedback has theoretical support in the work of Betts and Harshvardhan (1987), Senior and Mitchell (1993), and Tsushima et al. (2006) and observational support from Feigelson (1978), Somerville and Remer (1984), and Mace et al. (2001).

(iii) A common feature to the CMIP3 GCMs is an overall decrease in mid and low-level cloud amount equatorward of about 50°, an increase in high cloud amount along the equator, and an increase in cloud amount at most vertical levels poleward of 50°. These anomalies roughly track the anomalous relative humidity distribution [cf. Fig. 10.10 of Meehl et al. (2007) and Fig. 2 of Sherwood et al. (2010)]. The decrease (increase) in cloud fraction on the equatorward (poleward) flank of the midlatitudes is consistent with a poleward-shifted storm track. That a dry model forced only with a rising extratropical tropopause produces a poleward-shifted jet and storm track (Lorenz and DeWeaver 2007) implies that such features produced by GCMs (Hall et al. 1994; Yin 2005; Wu et al. 2010) and the cloud anomalies that accompany them are believable. Zelinka et al. (2012) calculated that these cloud amount anomalies contribute to a positive SW low-latitude cloud feedback and negative high-latitude cloud feedback, the latter reinforcing the strongly negative high-latitude SW optical depth feedback.

Third, the factor of 2 difference in land fraction in the NH compared with the SH and the much larger capacity of the ocean to store heat compared with land implies that transient warming will be much less in southern mid-to-high latitudes than in the north.

6. Change in surface fluxes over the twenty-first century

We now take a surface perspective and assess the change in surface fluxes between the end and the beginning of the twenty-first century. This will allow for partitioning of the implied poleward energy transport between ocean and atmosphere, as atmospheric transport anomalies depend only on atmospheric net heating anomalies. Figure 5 shows the sensitivity of the surface fluxes to global-mean temperature change. We have taken into account a surface cooling term caused by anomalous absorption of latent heat of fusion in the melting of snow but do not show it here, as it is a very small term at all latitudes. Note that positive values represent anomalous fluxes *into* the atmosphere. Transient global warming is associated with a net increase in the flux of energy into the surface of about 0.4 W m^{-2} K^{-1}, with generally larger fluxes into the surface at higher latitudes. One can think of this anomalous surface flux as a negative feedback on transient global warming. Ultimately, this term approaches zero as the climate equilibrates on the time scale of deep ocean mixing (Solomon et al. 2009).

Changes in absorption of SW radiation by increased atmospheric water vapor as well as changes in SW cloud radiative forcing that accompany greenhouse warming result in a slight decrease in global-mean net SW heating of the surface, though with considerable intermodel spread (Fig. 5a). An interesting feature is the consistent reduction in SW heating of the surface over the Southern Ocean.

Enhanced downwelling longwave radiation at the surface (i.e., LW cooling of the atmosphere; not shown) increases more than does upwelling LW emission from the surface (not shown) with global temperature rise, though both increase dramatically and with very little intermodel spread (Fig. 5b). Net LW fluxes actually cool the surface over many regions of the subtropical continents (not shown). Large anomalies in net atmospheric LW emission to the surface occur for almost every model at nearly every latitude but especially in the warm, moist tropics.

The net radiative flux anomaly at the surface is dominated by LW flux changes, as the ''back radiation'' from the atmosphere increases dramatically over the course of the century (Fig. 5c). One notable exception is the Southern Ocean region, where SW flux changes due to clouds reduce the net heating of the surface over a narrow latitudinal band.

Enhanced radiative heating of the surface is almost completely compensated by an increase in evaporation (anomalously positive latent heat flux from surface to atmosphere) at almost every latitude (Fig. 5d), though the intermodel variance in this flux is quite large. Anomalous surface-to-atmosphere latent heat fluxes are robustly negative in the Southern Ocean region, where the air–sea humidity gradient is reduced. The peak increase in latent heat flux to the atmosphere occurs at about 15°S in the ensemble mean, for reasons that remain to be investigated.

In the zonal mean, surface-to-atmosphere sensible heat flux anomalies are negative everywhere except over the poles, indicating that the atmosphere anomalously heats the surface at most latitudes as the planet warms (Fig. 5e). However, the full spatial pattern (not shown) indicates that the sensible heat flux anomalies are into the atmosphere over continents, where the surface temperature increases more rapidly than the overlying atmosphere. Again, the Southern Ocean stands out as a prominent area of anomalous sensible heat transfer from atmosphere to ocean, though the NH midlatitudes and subpolar latitudes also exhibit this feature to a lesser extent.

In general, net surface flux anomalies increase with latitude, exhibiting a minimum in low latitudes and large anomalous fluxes into the subpolar ocean (Fig. 5f). A dominant feature in the net surface flux sensitivity is a net downward flux of energy of about 2 W m^{-2} K^{-1} that

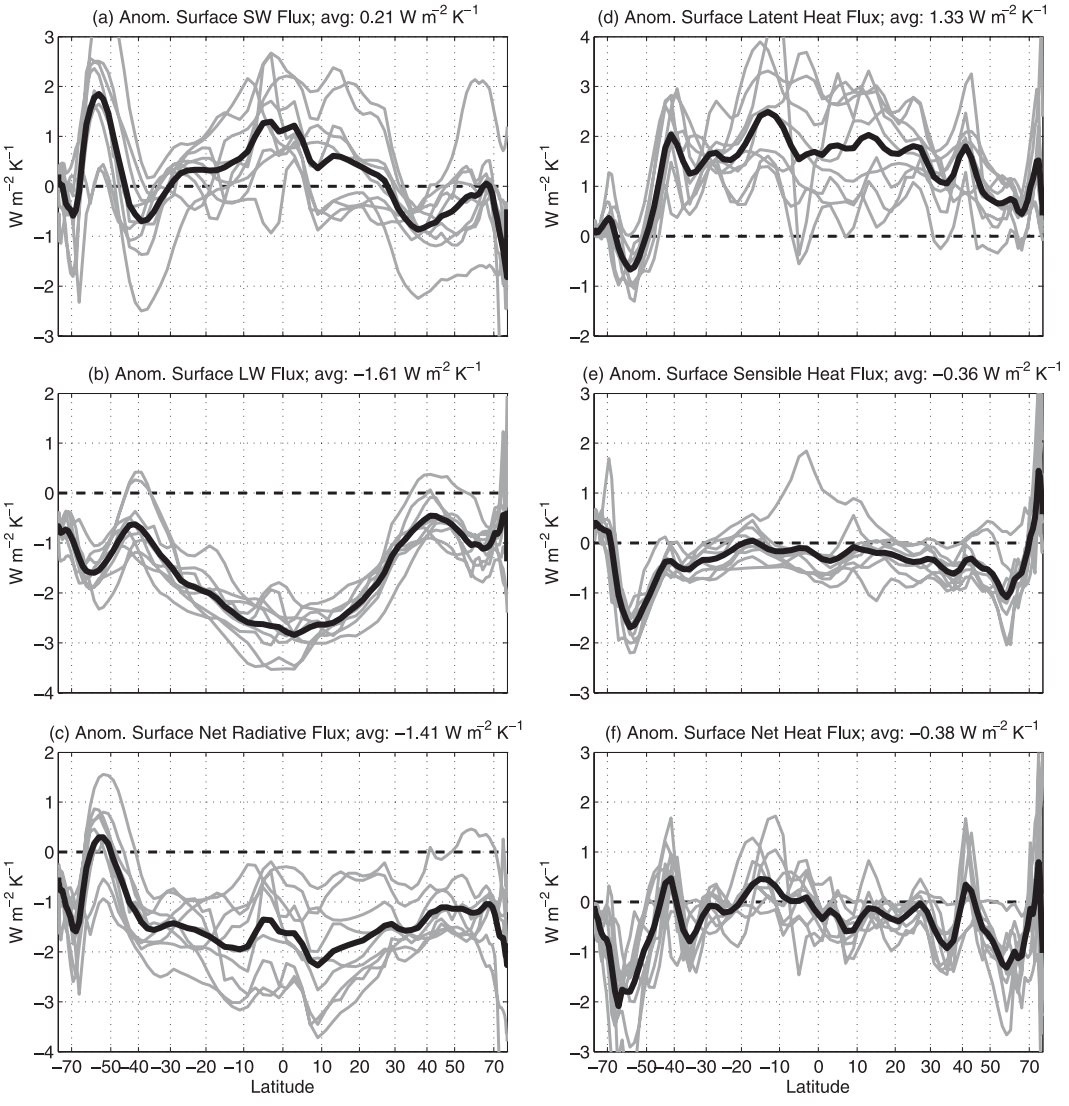

FIG. 5. Changes in surface (a) SW radiation, (b) LW radiation, (c) net radiation, (d) latent heat flux, and (e) sensible heat flux, along with (f) the sum of all terms over the twenty-first century, expressed per unit of global-mean temperature change. Positive anomalies represent anomalous fluxes *into* the atmosphere. Each of the nine models is represented by an individual gray line, and the thick black line represents the multimodel mean. Note that the vertical axis limits vary among panels, but all span a range of 6 W m^{-2} K^{-1}.

is concentrated in the southern extratropics. The largest part of this comes from the net downward flux of sensible heat from the atmosphere to the surface, but the net downward flux of latent heat and LW radiation also contributes. The Southern Ocean feature is present in all the models, though with different magnitudes and latitudes of peak heat uptake. This feature makes physical sense considering the vigorous vertical oceanic mixing that brings cold water to the surface and facilitates anomalous sensible heat transfer from atmosphere to ocean.

Broadly speaking, the surface flux anomaly structure mimics that of the TOA flux anomaly, resulting in a preferential heating of the tropical atmosphere relative to the high latitudes. This has important implications for the partitioning of energy fluxes between ocean and atmosphere as the planet warms. Specifically, the surface flux changes require that the atmospheric poleward heat flux increase more than the total poleward heat flux, as the ocean effectively transports less. This is discussed in greater detail in the next section.

7. Poleward energy flux sensitivity to feedback processes

Climatologically, regions of TOA energy surplus do not warm continuously while regions of energy deficit

cool continuously; rather the atmosphere and oceans transport energy from surplus to deficit regions (e.g., Vonder Haar and Oort 1973; Trenberth and Solomon 1994; Trenberth and Caron 2001; Trenberth and Stepaniak 2003). Anomalous meridional energy fluxes by the climate system perform the analogous role under global warming, diverging energy from regions in which feedbacks amplify the radiative forcing and converging energy into regions in which feedbacks dampen the radiative forcing. We have shown that the radiative kernel allows one to decompose the change in net TOA radiation at every location into the individual components causing the change. Here, we take the latitudinal structure of each component's radiation anomaly and calculate its implied poleward energy transport anomaly. This is done using a polar cap integration in which the anomalous energy flux across a latitude circle is equal to the TOA radiation anomaly within the polar cap extending to that latitude [cf. Eq. (2.21) of Hartmann (1994)]:

$$F'(\phi) = \int_{-\pi/2}^{\phi}\int_{0}^{2\pi} R'(\lambda,\phi)a^2\cos\phi\, d\lambda\, d\phi, \qquad (3)$$

where $F'(\phi)$ is the anomalous northward energy flux across a latitude circle, ϕ is latitude, λ is longitude, a is the radius of the earth, and $R'(\lambda, \phi)$ is the anomalous TOA radiative flux anomaly due to an individual feedback component with its global-mean value subtracted out. Negative anomalous net integrated TOA radiation within the polar cap (i.e., a net energy deficit anomaly at the TOA) implies an anomalous poleward flux of energy across the latitude circle into the cap.

We can also partition the net poleward energy transport between the atmosphere and ocean by taking into account the anomalous surface fluxes that accompany transient warming (discussed in the previous section). The implied atmospheric poleward transport is simply given as

$$F'_{\mathrm{atm}}(\phi) = \int_{-\pi/2}^{\phi}\int_{0}^{2\pi} [R'(\lambda,\phi) + F'_{\mathrm{sfc}}(\lambda,\phi)]a^2\cos\phi\, d\lambda\, d\phi, \qquad (4)$$

where $F'_{\mathrm{atm}}(\phi)$ is the anomalous northward atmospheric energy flux across a latitude circle, and $F'_{\mathrm{sfc}}(\lambda, \phi)$ is the anomalous surface flux anomaly with its global-mean value subtracted out. In Fig. 6 we plot the anomalous poleward transports that are implied by each feedback process and by the change in surface fluxes over the course of the century. The thick dashed line in panel (f) is the implied atmospheric energy flux anomaly due to the sum of TOA and surface flux anomalies produced by the models rather than inferred using the kernels. It is provided as measure of the fidelity with which the TOA flux anomalies computed in Eq. (1) can reproduce the implied poleward heat transport anomalies in the models and is discussed in detail below.

Taken alone, atmospheric and surface temperature anomalies that accompany global warming result in a huge radiative loss of energy to space in the tropics and at high northern latitudes (Fig. 3a). This requires anomalous northward energy flux by the climate system at nearly every latitude, implying that such a warming structure requires net flux from the SH to the NH (Fig. 6a). Large energy flux convergence into the tropics is required due to anomalous emission from the warmer upper troposphere.

Water vapor feedback, which acts to preferentially heat the tropics, implies a nearly hemispherically symmetric anomalous poleward energy flux that diverges energy from the deep tropics (Fig. 6b). This strongly opposes the anomalous energy flux convergence into the tropics that is implied by the temperature feedback.

Implied anomalous transport due to the cloud feedback exhibits considerable intermodel spread but is generally symmetric about the equator, requiring poleward flux in each hemisphere (Fig. 6d). Unlike the water vapor feedback, which decreases roughly monotonically with latitude, the cloud feedback remains positive until about 50° in either hemisphere, at which point it exhibits a rather sharp decrease with latitude (Fig. 3d). This results in an anomalous poleward transport due to clouds that peaks at higher latitudes than does the transport due to water vapor. Weaver (2003) speculated that changes in extratropical cloud radiative forcing that accompany storm track shifts in a warm climate could have a large influence on poleward energy flux; here, we show that radiative anomalies due to modeled cloud changes do indeed require enhanced poleward energy flux.

Surface albedo feedbacks require reduced poleward energy flux in each hemisphere but are much smaller at nearly every latitude than other individual implied transports (Fig. 6e). This is a slightly counterintuitive result, considering that one might expect the albedo feedback to be associated with enhanced flux of heat to the poles, where it can go into melting snow and ice. However, we are showing here the poleward energy flux anomalies due to albedo feedback alone, which preferentially heats the poles and implies a requirement for less horizontal energy flux convergence into the polar area.

In a similar manner to the implied transport due to clouds and water vapor feedbacks, the anomalous surface fluxes require enhanced poleward transport by the atmosphere. Because the atmosphere warms faster than the ocean at high latitudes, the ocean provides less heat to the atmosphere in high latitudes and therefore the

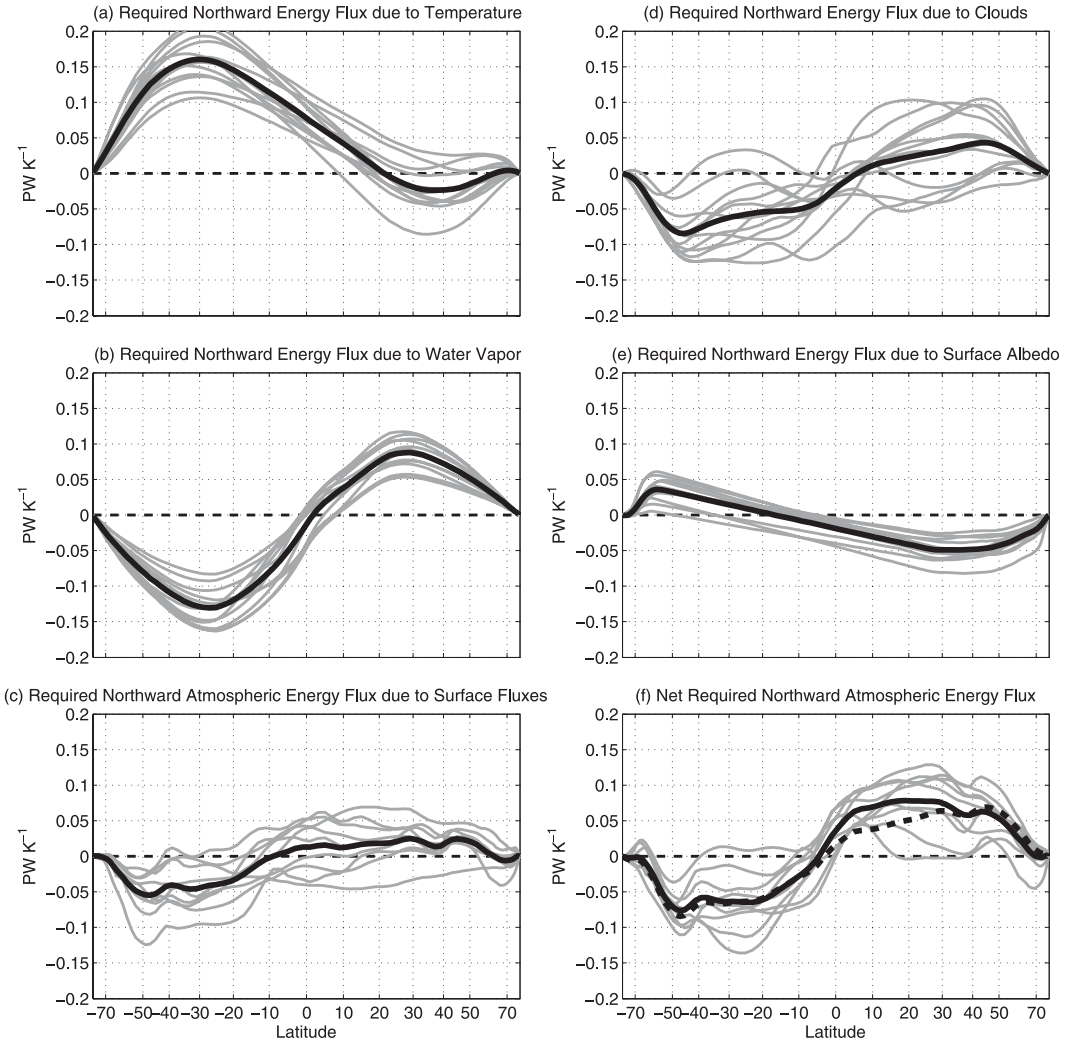

FIG. 6. Implied northward meridional energy flux anomalies in the climate system due to (a) temperature, (b) water vapor, (d) cloud, and (e) surface albedo feedbacks, and the implied *atmospheric* northward energy flux anomaly due to (c) anomalous surface fluxes and (f) the sum of TOA and surface heat flux anomalies. The thick dashed line in (f) is the implied flux due to the sum of TOA and surface flux anomalies produced by the models rather than inferred using the kernels.

atmosphere must carry more energy poleward (Fig. 6c). In other words, the latitudinal structure of anomalous surface fluxes tends to amplify the latitudinal structure of TOA radiative fluxes, thereby requiring the atmosphere to transport more energy in a warming climate.

Figure 7a shows the model ensemble average TOA flux anomalies with the global mean removed, and Fig. 7b shows the meridional flux anomalies required by the gradients in TOA flux anomalies. The net radiative plus surface flux shows a peak positive anomaly in the equatorial region that, as already noted, requires an enhanced meridional flux away from the equator. The primary contributors to this equatorial peak are water vapor and longwave cloud feedbacks. Other notable features are the large transitions from net positive atmospheric heating anomalies on the equatorial side of the midlatitudes to net negative atmospheric heating anomalies on the poleward side of the midlatitudes. In both hemispheres, the midlatitude cooling anomaly is about twice as large as the heating anomaly, and the magnitude of this latitudinal fluctuation is about twice as large in the SH than in the NH. These are caused by the combination of strong negative cloud feedbacks and large anomalous fluxes of heat into the ocean. It is interesting that the subpolar atmosphere loses heat both out of its top by way of strong negative cloud feedbacks as well as out of its bottom by way of strong sensible and longwave fluxes to the surface. This feature is larger in the SH because the cloud

feedback and anomalous surface flux signatures are more sharply defined and collocated than their NH counterparts and because the opposing positive surface albedo feedback extends farther equatorward in the NH. Required poleward flux anomalies reflect these midlatitude features, exhibiting secondary peaks in the midlatitudes such that narrow latitude bands experience heat flux divergence while the poles receive enhanced energy flux convergence.

The temperature feedback shows a strong hemispheric asymmetry with more positive values (relative to the global mean) in the SH than in the NH. The temperature feedback asymmetry is, as always, offset somewhat by the water vapor feedback. On the equator, however, the northward energy flux change associated with temperature is partially offset equally by that associated with the water vapor, cloud, and surface albedo feedbacks, leaving a small residual northward net flux change. This net northward energy flux at the equator must be accomplished by anomalous northward dry static energy transport by a southward-shifted Hadley Circulation (Kang et al. 2008, 2009). This cross-equator anomalous flux is not present in the ensemble-mean results of Held and Soden (2006) or Hwang and Frierson (2010), however, suggesting that a southward-shifted ITCZ is not robust across models. In each hemisphere, the peak atmospheric poleward energy flux anomalies are roughly 0.08 PW per degree of global-mean temperature increase. Considering the global warming simulated by the models is ~3.25 K, these flux changes are 10%–20% as large as the mean atmospheric flux in low latitudes [cf. Fig. 7 of Trenberth and Caron (2001)].

Ensemble-mean implied poleward energy transport anomalies in the climate system are shown in Fig. 8. The "ocean" term is not the change in poleward oceanic energy flux, but rather the sum of the change in oceanic poleward flux and heat storage computed by assuming all net surface fluxes into the surface go into either transport or storage in the ocean. Also shown is the poleward energy transport anomaly computed using the ensemble-mean TOA flux anomalies produced by the models (i.e., archived directly by the model rather than implied from the radiative kernel calculation).

It is clear from Fig. 8 that oceanic poleward energy transport and storage anomalies act in the opposite sense to what is required at the TOA, thereby placing more of the burden of transporting energy to the pole on the atmosphere. As summarized in Meehl (2007), several studies (e.g., Hazeleger 2005; Hu et al. 2004) have found robust reductions in oceanic poleward heat transport associated with reductions in the strength of the Atlantic meridional overturning circulation in coupled GCMs over the course of the twenty-first century for a variety

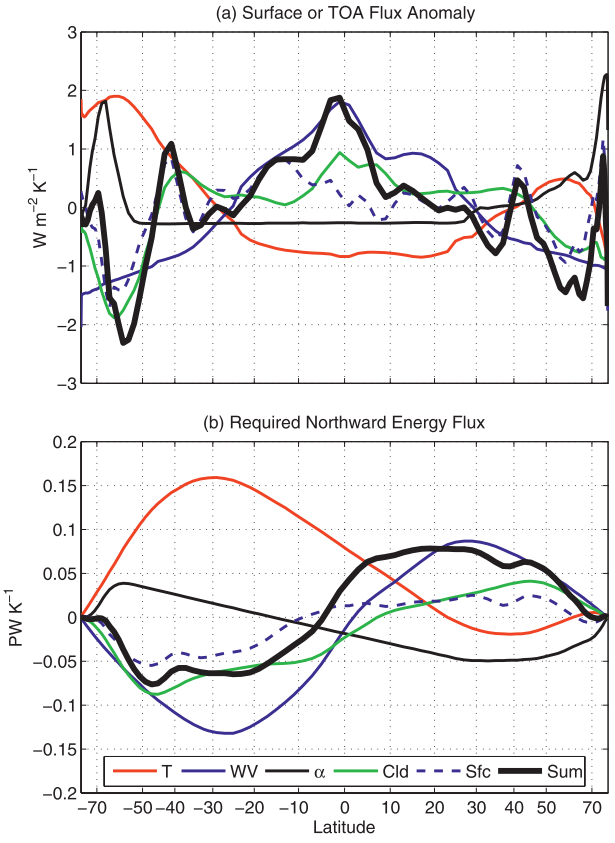

FIG. 7. (a) Multimodel-mean TOA and surface flux anomalies and (b) implied northward meridional energy flux anomalies due to changes in (red) temperature, (solid blue) water vapor, (thin black) surface albedo, (green) clouds, (dashed blue) surface fluxes, and (thick black) net fluxes into the atmosphere. The TOA and surface flux anomalies are plotted as anomalies from their global means.

of increasing CO_2 scenarios. Moreover, Hu et al. (2004) found a decrease in oceanic poleward heat transport in the Atlantic basin south of 60°N and an increase north of 60°N in the National Center for Atmospheric Research (NCAR) Parallel Climate Model (PCM), with magnitudes similar to those shown in Fig. 8. Comparing Figs. 3a and 3b of Hwang et al. (2011) [which is the corrected version of Fig. 11 of Held and Soden (2006)], it is clear that increases in atmospheric heat transport that accompany a warming climate are more pronounced in fully coupled GCMs with dynamic oceans because of the latter's ability to sequester more heat from the high-latitude atmosphere.

Clearly there are differences between the implied poleward fluxes estimated using the kernel technique and derived directly from the models' TOA fluxes, especially in the NH. This can be attributed to errors associated with Eq. (1) discussed in section 4. The kernel-derived fluxes imply more (less) poleward transport in low (high) latitudes of the NH than the directly computed TOA flux

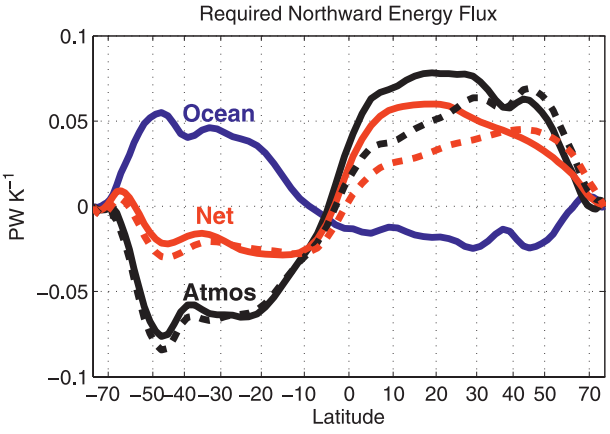

FIG. 8. The implied changes in (red solid) net poleward energy transport by the climate system, partitioned into components due to changes in (black) atmosphere transport and (blue) the sum of oceanic transport and storage. Also provided in the black and red dashed lines are the atmospheric and net energy transport anomalies, respectively, computed directly from the ensemble-mean TOA flux anomalies (i.e., without use of the radiative kernels). Note that the solid black curve is the same as in Fig. 7.

anomalies. In the ensemble mean, actual TOA SW anomalies are more positive than those computed with the kernel over the majority of the NH, especially in midlatitudes, and much more negative over the Arctic than those computed with the kernel, possibly indicating a strong local reduction of reflective aerosols in the midlatitudes that is not captured by our simple use of a spatially invariant G. In the ensemble mean, the actual TOA LW anomalies are more negative at the equator and pole and more positive in midlatitudes than those computed with the kernels. It is unclear why this structure emerges, but it may also be related to changes in absorbing aerosol that are very regionally dependent. Such unaccounted-for anomalous heating of NH midlatitudes relative to the tropics and poles would require less poleward flux at low latitudes and more poleward flux at high latitudes, which is what we see when comparing the solid and dashed curves. Clearly, uncertainties in both the forcing and feedback estimates impact the implied anomalous poleward energy flux that accompanies global warming, especially in the NH.

Several important conclusions are drawn from this section. First, poleward energy transport in a warming climate is enhanced owing to the presence of feedbacks (e.g., Wu et al. 2010). Second, feedbacks that may be considered ''local'' from the TOA perspective have relevance at all latitudes because of their induced circulation responses (e.g., Chiang and Bitz 2005; Yoshimori and Broccoli 2008; Kang et al. 2008, 2009; Fletcher et al. 2009; Hwang and Frierson 2010). Third, locally large positive feedbacks need not imply locally large surface temperature changes if compensated by anomalous horizontal energy flux divergence. Finally, the atmosphere must perform more of the net poleward energy transport in the presence of an underlying ocean (e.g., Held and Soden 2006).

8. Summary, discussion, and implications

Positive feedbacks in the climate system act to reduce the efficiency with which the planet comes back into radiative equilibrium following a sustained radiative forcing due to long-lived greenhouse gases. This results in a planet that must warm more than if there were no positive feedbacks present. We have shown in this paper that these feedbacks have rich spatial structures that—by conservation of energy—have implications for poleward heat transport in a warming climate. In general, feedbacks act to preferentially heat the tropics relative to the poles, effectively strengthening the mean state equator-to-pole energy gradient and requiring the climate system to transport more heat poleward, in agreement with previous studies (e.g., Wu et al. 2010, Hwang and Frierson 2010).

A particular strength of this study is the use of radiative kernels to partition the net feedback and its implied poleward heat transport anomalies among its individual components. In so doing, we have shown that enhanced poleward heat transport is necessitated primarily by the decrease with latitude of water vapor and cloud feedbacks. Furthermore, we can attribute most of the intermodel spread in poleward energy flux changes to spread in SW cloud feedback estimates, a result also found by Hwang and Frierson (2010).

The ocean has tremendous thermal inertial in high latitudes, where the ocean mixes to depth and can access the huge heat capacity of the deep ocean. This impedes the warming of the upper ocean in high latitudes relative to other latitudes and facilitates large anomalous surface heat fluxes out of the high latitude atmosphere as the planet warms. The surface flux anomalies amplify the latitudinal gradient of heat loss from the atmosphere and require that the atmosphere perform more of the poleward energy transport and the ocean less.

We have argued that several of the gross features of the climate response can be expected from basic principles, namely that the water vapor feedback exhibit a maximum at low latitudes where OLR is most sensitive to water vapor perturbations and where the greatest moistening occurs, that the cloud feedback be positive at low latitudes due to the rising of tropical cloud tops and negative at high latitudes due to a shifted storm track and/or a brightening of clouds (due to increased liquid water content), that LW emission from the NH be larger

than that from the SH because of the hemispheric gradient in surface warming that can largely be attributed to continental geography (i.e., twice as much ocean in the SH), and that anomalous oceanic heat uptake preferentially occur at high latitudes, where vigorous mixing and deep water formation are most efficient. In sum, these features give us confidence that a robust increase in poleward energy transport by the climate system, with atmospheric transport increasing at the expense of oceanic transport, is realistic and makes sense intuitively.

Finally, this study has illuminated several interesting features of the climate system.

Horizontal energy transport, radiative heating, and surface warming are intimately coupled such that regions that are anomalously heated by radiation (i.e., by forcings and feedbacks) are anomalously cooled by dynamics (i.e., by meridional energy transport). Thus one can think of dynamical heating as a negative feedback on radiative heating at local scales. This is an important result that implies, for example, that models with large surface albedo feedbacks need not be models having large anomalous energy flux convergence into the high latitudes, a point also made by Hwang and Frierson (2010).

It is also noteworthy that although each feedback has particular regions in which it is most pronounced (e.g., at high latitudes for surface albedo feedback), it impacts the implied poleward transport at all latitudes. Thus, processes occurring in remote regions of the planet influence the energy budget throughout the climate system, even if they are not important (from a TOA perspective) locally. This point was emphasized by Fletcher et al. (2009) in the response of atmospheric circulation to snow albedo feedback on NH land as well as by Chiang and Bitz (2005), Yoshimori and Broccoli (2008), Kang et al. (2008), and Kang et al. (2009) in the movement of the ITCZ due to extratopical forcings. Kang et al. (2009) additionally showed that cloud and water vapor feedbacks cause a larger atmospheric response to hemispherically asymmetric imposed radiative forcing than in an idealized model (Frierson et al. 2006) in which those feedbacks are suppressed, a result consistent with our findings.

Another point that is perhaps generally unappreciated is that anomalies in meridional energy transport depend on latitudinal anomalies of feedbacks from their global-mean values rather than the magnitudes of their global-mean values. It thus follows that feedbacks that are relatively unimportant for climate sensitivity because they globally integrate to a small number can hypothetically be very important for anomalous energy transport. This is obvious from the results of Kang et al. (2008) and Kang et al. (2009), who showed that a hemispherically asymmetric radiative forcing anomaly that integrated to zero globally caused large changes in poleward energy flux. Although we find in this study that the largest individual contributors to anomalous energy transport tend to also be the largest globally integrated feedbacks, it is interesting to recognize that this need not be the case.

Finally, the Southern Ocean region, in which the atmosphere and ocean strongly influence each other, stands out in this study as one in which the transient response of the climate is dramatic. Russell et al. (2006b), Russell et al. (2006a), Delworth and Zeng (2008), Toggweiler and Russell (2008), and Sen Gupta et al. (2009) have emphasized the importance of surface westerlies over the Southern Ocean as well as their poleward shift and intensification in allowing for increased oceanic heat uptake in the face of increased upper ocean stratification during transient warming. They find that the intermodel spread in Southern Ocean heat uptake is in large part attributable to the response of surface westerlies in this region, which themselves are likely to be affected both in strength and location by the requirements of poleward energy transport set in place by TOA and surface flux anomalies. Caution is provided, however, by Boning et al. (2008) and Farneti and Delworth (2010), who suggest that the large sensitivity of Southern Ocean circulation to surface winds may be exaggerated in coarse-resolution ocean models that do not resolve eddies. Regardless, one could conceive of possible feedbacks (in the generic sense) involving a poleward-shifted storm track, the latitudinal gradient of cloud feedbacks, the strength of the surface winds over the Southern Ocean, upwelling and attendant heat uptake in the Southern Ocean, and meridional temperature gradients, all of which likely interact with one another in ways that—to our knowledge—have not been adequately explored. The Southern Ocean's importance in taking up both heat and anthropogenic CO_2 (Mignone et al. 2006) argues for more extensive investigation into such regional feedbacks.

Acknowledgments. This research was supported by NASA Grant NNX09AH73G, NASA Earth and Space Science Fellowship NNX06AF69H, and by the Lawrence Livermore National Laboratory Institutional Postdoc Program. We acknowledge the international modeling groups, the Program for Climate Model Diagnosis and Intercomparison (PCMDI), and the WCRP's Working Group on Coupled Modelling (WGCM) for their roles in making available the WCRP CMIP3 multimodel dataset. Support of this dataset is provided by the Office of Science, U.S. Department of Energy. We thank Brian Soden for providing the radiative kernels, Dargan Frierson, Yen-Ting Hwang, Angie Pendergrass, Kyle Armour, Aaron Donohoe, and Chris Bretherton for useful discussion and suggestions for improvement,

and Marc Michelsen for computer support. This work was performed under the auspices of the U.S. Department of Energy by Lawrence Livermore National Laboratory under Contract DE-AC52-07NA27344.

REFERENCES

Andrews, T., and P. M. Forster, 2008: CO_2 forcing induces semi-direct effects with consequences for climate feedback interpretations. *Geophys. Res. Lett.,* **35,** L04802, doi:10.1029/2007GL032273.

Betts, A. K., and Harshvardhan, 1987: Thermodynamic constraint on the cloud liquid water feedback in climate models. *J. Geophys. Res.,* **92,** 8483–8485.

Boning, C. W., A. Dispert, M. Visbeck, S. R. Rintoul, and F. U. Schwarzkopf, 2008: The response of the Antarctic Circumpolar Current to recent climate change. *Nature,* **1,** 864–869.

Cess, R. D., 1975: Global climate change—Investigation of atmospheric feedback mechanisms. *Tellus,* **27,** 193–198.

Chang, F.-L., and J. A. Coakley, 2007: Relationships between marine stratus cloud optical depth and temperature: Inferences from AVHRR observations. *J. Climate,* **20,** 2022–2036.

Chiang, J. C. H., and C. M. Bitz, 2005: The influence of high latitude ice on the position of the marine intertropical convergence zone. *Climate Dyn.,* **25,** 477–496, doi:10.1007/s00382-005-0040-5.

Colman, R., 2003: A comparison of climate feedbacks in general circulation models. *Climate Dyn.,* **20,** 865–873.

——, and B. McAvaney, 2011: On tropospheric adjustment to forcing and climate feedbacks. *Climate Dyn.,* **36,** 1–10.

Delworth, T. L., and F. Zeng, 2008: Simulated impact of altered Southern Hemisphere winds on the Atlantic meridional overturning circulation. *Geophys. Res. Lett.,* **35,** L20708, doi:10.1029/2008GL035166.

Dong, B., J. M. Gregory, and R. T. Sutton, 2009: Understanding land–sea warming contrast in response to increasing greenhouse gases. Part I: Transient adjustment. *J. Climate,* **22,** 3079–3097.

Farneti, R., and T. L. Delworth, 2010: The role of mesoscale eddies in the remote oceanic response to altered Southern Hemisphere winds. *J. Phys. Oceanogr.,* **40,** 2348–2354.

Feigelson, E. M., 1978: Preliminary radiation model of a cloudy atmosphere. Part I: Structure of clouds and solar radiation. *Beitr. Phys. Atmos.,* **51,** 203–229.

Fletcher, C. G., P. J. Kushner, A. Hall, and X. Qu, 2009: Circulation responses to snow albedo feedback in climate change. *Geophys. Res. Lett.,* **36,** L09702, doi:10.1029/2009GL038011.

Frierson, D. M. W., I. M. Held, and P. Zurita-Gotor, 2006: A gray-radiation aquaplanet moist GCM. Part I: Static stability and eddy scale. *J. Atmos. Sci.,* **63,** 2548–2566.

Gregory, J., and M. Webb, 2008: Tropospheric adjustment induces a cloud component in CO2 forcing. *J. Climate,* **21,** 58–71.

Hall, N. M. J., B. J. Hoskins, P. J. Valdes, and C. A. Senior, 1994: Storm tracks in a high-resolution GCM with doubled carbon dioxide. *Quart. J. Roy. Meteor. Soc.,* **120,** 1209–1230.

Hansen, J., A. Lacis, D. Rind, G. Russell, P. Stone, I. Fung, R. Ruedy, and J. Lerner, Eds., 1984: *Climate Processes and Climate Sensitivity: Analysis of Feedback Mechanisms*. *Geophys. Monogr.,* Vol. 29, Amer. Geophys. Union, 130–163.

Hartmann, D. L., 1994: *Global Physical Climatology*. Academic Press, 411 pp.

——, and K. Larson, 2002: An important constraint on tropical cloud-climate feedback. *Geophys. Res. Lett.,* **29,** 1951, doi:10.1029/2002GL015835.

Hazeleger, W., 2005: Can global warming affect tropical ocean heat transport? *Geophys. Res. Lett.,* **32,** L22701, doi:10.1029/2005GL023450.

Held, I. M., and B. J. Soden, 2006: Robust responses of the hydrological cycle to global warming. *J. Climate,* **19,** 5686–5699.

Hu, A., G. A. Meehl, W. M. Washington, and A. Dai, 2004: Response of the atlantic thermohaline circulation to increased atmospheric CO_2 in a coupled model. *J. Climate,* **17,** 4267–4279.

Huybers, P., 2010: Compensation between model feedbacks and curtailment of climate sensitivity. *J. Climate,* **23,** 3009–3018.

Hwang, Y.-T., and D. M. W. Frierson, 2010: Increasing atmospheric poleward energy transport with global warming. *Geophys. Res. Lett.,* **37,** L24807, doi:10.1029/2010GL045440.

——, ——, B. J. Soden, and I. M. Held, 2011: Corrigendum. *J. Climate,* **24,** 1559–1560.

Joshi, M., J. Gregory, M. Webb, D. Sexton, and T. Johns, 2008: Mechanisms for the land/sea warming contrast exhibited by simulations of climate change. *Climate Dyn.,* **30,** 455–465.

Kang, S. M., I. M. Held, D. M. W. Frierson, and M. Zhao, 2008: The response of the ITCZ to extratropical thermal forcing: Idealized slab-ocean experiments with a GCM. *J. Climate,* **21,** 3521–3532.

——, D. M. W. Frierson, and I. M. Held, 2009: The tropical response to extratropical thermal forcing in an idealized GCM: The importance of radiative feedbacks and convective parameterization. *J. Atmos. Sci.,* **66,** 2812–2827.

Kushner, P. J., I. M. Held, and T. L. Delworth, 2001: Southern Hemisphere atmospheric circulation response to global warming. *J. Climate,* **14,** 2238–2249.

Lorenz, D. J., and E. T. DeWeaver, 2007: Tropopause height and zonal wind response to global warming in the IPCC scenario integrations. *J. Geophys. Res.,* **112,** D10119, doi:10.1029/2006JD008087.

Mace, G. G., E. E. Clothiaux, and T. P. Ackerman, 2001: The composite characteristics of cirrus clouds: Bulk properties revealed by one year of continuous cloud radar data. *J. Climate,* **14,** 2185–2203.

Meehl, G. A., and Coauthors, 2007: Global climate projections. *Climate Change 2007: The Physical Science Basis,* S. Solomon et al., Eds., Cambridge University Press, 747–845.

Mignone, B. K., A. Gnanadesikan, J. L. Sarmiento, and R. D. Slater, 2006: Central role of Southern Hemisphere winds and eddies in modulating the oceanic uptake of anthropogenic carbon. *Geophys. Res. Lett.,* **33,** L01604, doi:10.1029/2005GL024464.

Ramaswamy, V., and Coauthors, 2001: Radiative forcing of climate change. *Climate Change 2001: The Scientific Basis,* J. T. Houghton et al., Eds., Cambridge University Press, 350–416.

Roe, G. H., 2009: Feedbacks, timescales, and seeing red. *Annu. Rev. Earth Planet. Sci.,* **37,** 93–115.

——, and M. B. Baker, 2007: Why is climate sensitivity so unpredictable? *Science,* **318,** 629–632.

Russell, J. L., K. W. Dixon, A. Gnanadesikan, R. J. Stouffer, and J. R. Toggweiler, 2006a: The Southern Hemisphere westerlies in a warming world: Propping open the door to the deep ocean. *J. Climate,* **19,** 6382–6390.

——, R. J. Souffer, and K. W. Dixon, 2006b: Intercomparison of the Southern Ocean circulations in the IPCC coupled model control simulations. *J. Climate,* **19,** 4560–4575.

Santer, B. D., and Coauthors, 2003: Contributions of anthropogenic and natural forcing to recent tropopause height changes. *Science,* **301,** 479–483.

Sen Gupta, A., A. Santoso, A. S. Taschetto, C. C. Ummenhofer, J. Trevena, and M. H. England, 2009: Projected changes to the Southern Hemisphere ocean and sea ice in the IPCC AR4 climate models. *J. Climate,* **22,** 3047–3078.

Senior, C., and J. Mitchell, 1993: Carbon dioxide and climate: The impact of cloud parameterization. *J. Climate,* **6,** 393–418.

Sherwood, S. C., W. Ingram, Y. Tsushima, M. Satoh, M. Roberts, P. L. Vidale, and P. A. O'Gorman, 2010: Relative humidity changes in a warmer climate. *J. Geophys. Res.,* **115,** D09104, doi:10.1029/2009JD012585.

Shindell, D. T., H. Levy, M. D. Schwarzkopf, L. W. Horowitz, J.-F. Lamarque, and G. Faluvegi, 2008: Multimodel projections of climate change from short-lived emissions due to human activities. *J. Geophys. Res.,* **113,** D11109, doi:10.1029/2007JD009152.

Soden, B. J., and I. M. Held, 2006: An assessment of climate feedbacks in coupled ocean–atmosphere models. *J. Climate,* **19,** 3354–3360.

——, ——, R. Colman, K. M. Shell, J. T. Kiehl, and C. A. Shields, 2008: Quantifying climate feedbacks using radiative kernels. *J. Climate,* **21,** 3504–3520.

Solomon, S., G.-K. Plattner, R. Knutti, and P. Friedlingsteind, 2009: Irreversible climate change due to carbon dioxide emissions. *Proc. Natl. Acad. Sci. USA,* **106,** 1704–1709.

Somerville, R. C. J., and L. A. Remer, 1984: Cloud optical thickness feedbacks in the CO_2 climate problem. *J. Geophys. Res.,* **89** (D6), 9668–9672.

Sutton, R. T., B. Dong, and J. M. Gregory, 2007: Land/sea warming ratio in response to climate change: IPCC AR4 model results and comparison with observations. *Geophys. Res. Lett.,* **34,** L02701, doi:10.1029/2006GL028164.

Toggweiler, J. R., and J. Russell, 2008: Ocean circulation in a warming climate. *Nature,* **451,** 286–288.

Trenberth, K. E., and A. Solomon, 1994: The global heat balance: Heat transports in the atmosphere and ocean. *Climate Dyn.,* **10,** 107–134.

——, and J. M. Caron, 2001: Estimates of meridional atmosphere and ocean heat transports. *J. Climate,* **14,** 3433–3443.

——, and D. P. Stepaniak, 2003: Seamless poleward atmospheric energy transports and implications for the Hadley circulation. *J. Climate,* **16,** 3706–3722.

Tselioudis, G., and W. B. Rossow, 1994: Global, multiyear variations of optical thickness with temperature in low and cirrus clouds. *Geophys. Res. Lett.,* **21,** 2211–2214.

——, ——, and D. Rind, 1992: Global patterns of cloud optical thickness variation with temperature. *J. Climate,* **5,** 1484–1495.

Tsushima, Y., and Coauthors, 2006: Importance of the mixed-phase cloud distribution in the control climate for assessing the response of clouds to carbon dioxide increase: A multi-model study. *Climate Dyn.,* **27,** 113–126.

Vonder Haar, T. H., and A. H. Oort, 1973: New estimate of annual poleward energy transports by Northern Hemisphere oceans. *J. Phys. Oceanogr.,* **3,** 169–172.

Weaver, C. P., 2003: Efficiency of storm tracks an important climate parameter? The role of cloud radiative forcing in poleward heat transport. *J. Geophys. Res.,* **108,** 4018, doi:10.1029/2002JD002756.

Wu, Y., M. Ting, R. Seager, H.-P. Huang, and M. Cane, 2010: Changes in storm tracks and energy transports in a warmer climate simulated by the GFDL CM2.1 model. *Climate Dyn.,* 1–20, doi:10.1007/s00382-010-0776-4.

Yin, J. H., 2005: A consistent poleward shift of the storm tracks in simulations of 21st century climate. *Geophys. Res. Lett.,* **32,** L18701, doi:10.1029/2005GL023684.

Yoshimori, M., and A. J. Broccoli, 2008: Equilibrium response of an atmosphere–mixed layer ocean model to different radiative forcing agents: Global and zonal mean response. *J. Climate,* **21,** 4399–4423.

Zelinka, M. D., and D. L. Hartmann, 2010: Why is longwave cloud feedback positive? *J. Geophys. Res.,* **115,** D16117, doi:10.1029/2010JD013817.

——, S. A. Klein, and D. L. Hartmann, 2012: Computing and partitioning cloud feedbacks using cloud property histograms. Part II: Attribution changes in cloud amount, altitude, and optical depth. *J. Climate,* in press.